Available online at www.sciencedirect.com

SciVerse ScienceDirect

Geochimica et Cosmochimica Acta 93 (2012) 262–277

Geochimica et Cosmochimica Acta

www.elsevier.com/locate/gca

U(VI) sorption on montmorillonite in the absence and presence of carbonate: A macroscopic and microscopic study

M. Marques Fernandes [a,*,1], B. Baeyens [a], R. Dähn [a], A.C. Scheinost [b], M.H. Bradbury [a]

[a] Paul Scherrer Institut, Laboratory for Waste Management, 5232 Villigen PSI, Switzerland
[b] Helmholtz Zentrum Dresden-Rossendorf e.V. (HZDR), Institute of Resource Ecology, 01314 Dresden, Germany

Received 7 February 2011; accepted in revised form 5 April 2012; available online 17 April 2012

Abstract

The mechanism of U(VI) sorption on montmorillonite (Na-SWy-1) in the absence and presence of carbonate was investigated through a combination of different approaches: macroscopic sorption experiments, surface complexation modelling using the 2 Site Protolysis Non Electrostatic Surface Complexation and Cation Exchange sorption model and Extended X-ray Absorption Fine Structure (EXAFS) spectroscopy. U(VI) sorption measurements were performed in the absence of carbonate at fixed ionic strength (0.1 M $NaClO_4$) as a function of pH at U(VI) trace concentration ($\sim 9 \times 10^{-8}$ M) and as a function of U(VI) concentration ($\sim 10^{-7}$–10^{-4} M) at a fixed pH (5, 6.8 and 8). In the presence of carbonate, experiments were carried out in equilibrium with atmospheric pCO_2 and in 1, 3 and 5 mM $NaHCO_3$. The pH dependent sorption measurements at trace concentration in the absence of carbonate were modelled by considering the formation of the following surface species, $\equiv S^{S}OUO_2^+$, $\equiv S^{S}OUO_2OH^0$, $\equiv S^{S}OUO_2(OH)_2^-$ and $\equiv S^{S}OUO_2(OH)_3^{2-}$ on the strong sites. From the isotherms the formation of $\equiv S^{W1}OUO_2^+$ and $\equiv S^{W1}OUO_2OH^0$ on the weak sites was inferred. Two additional surface complexes on the strong sites, $\equiv S^{S}OUO_2CO_3^-$ and $\equiv S^{S}OUO_2(CO_3)_2^{3-}$ and one surface complex on the weak sites, $S^{W1}OUO_2CO_3^-$, were necessary to reproduce the sorption data obtained in the presence of carbonate. The EXAFS measurements did not allow to verify the formation of ternary uranyl-carbonate complexes on the montmorillonite surface. However, the obtained fit results, *i.e.* splitting of the equatorial oxygen shell, one Si/Al shell at ~3.09 Å and one Si/Al at ~3.29 Å or one Fe shell at ~3.42 Å, clearly indicate that under the given experimental conditions (pH, U(VI) loading) U(VI) forms inner-sphere surface complexes on montmorillonite edge sites via binding to aluminum octahedra and/or silicon tetrahedra.

1. INTRODUCTION

Uranium is an important environmental radioactive contaminant originating from activities such as uranium mining and nuclear facilities (Burns and Finch, 1999). The leaching of uranium mine and mill tailings has often resulted in the contamination of soils and aquifers through the development and migration of plumes with high levels of dissolved U (Bond et al., 2007). In deep geological concepts for the disposal of radioactive waste, the high level waste and spent fuel will be protected from contact with the groundwater for long times by the near field engineered multi barrier system (thick steel canisters, compacted bentonite backfill). Eventually, after the steel canisters have corroded away, groundwater will reach the waste and uranium will begin to dissolve slowly and be released into the engineered barrier system and then subsequently into the host rock.

Quantifying the transport of radioactive contaminants within aquifers, in soils or through rock formations relies on a detailed knowledge of the geochemistry of the system and of the radionuclide retention mechanisms along the migration pathways (sorption, incorporation, precipita-

* Corresponding author.
E-mail address: maria.marques@psi.ch (M. Marques Fernandes).
[1] Present address.

0016-7037/$ - see front matter © 2012 Elsevier Ltd. All rights reserved.
http://dx.doi.org/10.1016/j.gca.2012.04.017

tion. . ..). The retardation of radiocontaminants is strongly affected by their sorption/desorption behaviour at the mineral–water interface.

Clay minerals are major constituents in many soils and, potential argillaceous host rocks (containing 50 or more wt.% illite and illite/smectite mixed layers) for radioactive waste disposal. Bentonite (containing 75–90 wt.% montmorillonite) is a preferred material for backfilling and sealing high level radioactive waste repositories (Nagra, 2002). Retardation is especially effective in 2:1 type clay minerals (*e.g.* illite, montmorillonite) because of their large surface areas and their strong surface retention capacities.

The sorption of metal ions is strongly influenced by the geochemical conditions in the aquatic environment, *e.g.* ionic strength, Eh, pH, T, presence of organic or inorganic ligands and their complexation characteristics. Under oxidizing conditions uranium exists in its hexavalent oxidation state as the uranyl ion UO_2^{2+} and can form highly soluble aqueous complexes with many ligands present in groundwaters *e.g.* OH^-, F^-, SO_4^{2-}, PO_4^{3-} and CO_3^{2-}. Dissolved carbonate is particularly ubiquitous in surface and deep groundwaters and forms strong aqueous complexes with U(VI) (Guillaumont et al., 2003). The formation of such complexes can potentially lead to a decrease in sorption and thereby an increase in the migration rates of U(VI). A detailed understanding of the sorption processes over a wide range of conditions is essential for the development of predictive sorption models.

Several surface complexation models based on macroscopic sorption experiments have been developed to explain the adsorption behaviour of uranyl, particularly on montmorillonite (Zachara and McKinley 1993; McKinley et al. 1995; Turner et al. 1996; Pabalan and Turner 1997; Kim 2001; Kowal-Fouchard et al. 2004; Bradbury and Baeyens 2005). At low ionic strengths, uranyl is sorbing primarily to cation exchange sites in the interlayer below pH ~5 and to the edge sites (silanol and/or aluminol) above this pH. At high ionic strengths, cation exchange is strongly reduced and sorption is taking place from pH ~5 onwards mainly at the edge sites of montmorillonite.

The influence of carbonate on the sorption of uranyl on clay minerals has been reported less in the open literature. Pabalan and Turner (1997) and Bachmaf et al. (2008) investigated the sorption of U(VI) on montmorillonite and bentonite, respectively, in the presence of carbonate. These authors observed a sharp decrease of sorption at pH values above 6.5 and explained this behaviour by the formation of non sorbing negatively charged uranyl-carbonate complexes in solution.

Surface complexation reactions and their corresponding stability constants implemented in sorption models have a considerably higher credibility and reliability if they can be supported by structural data of the surface complexes obtained by spectroscopic methods. Extended X-ray Absorption Fine Structure (EXAFS) spectroscopy has been used to investigate the sorption mechanisms of uranyl on different clay minerals under different conditions in the absence of carbonate (Dent et al., 1992; Chisholm-Brause et al., 1994; Sylwester et al., 2000; Hennig et al., 2002; Catalano and Brown, 2005; Schlegel and Descostes, 2009). Depending on pH and U(VI) loading, these studies were able to differentiate between outer-sphere complexation *i.e.* cation exchange and inner-sphere complexation at the edge sites of clay minerals. Outer-sphere complexation is characterized by EXAFS spectra which are very similar to that of the UO_2^{2+} aquo ion, whereas inner-sphere complexation is characterized by the splitting of the equatorial shells and/or the backscattering contributions from neighbouring atoms such as Si, Al or Fe. Catalano et al. (2005) investigated the sorption of U(VI) on montmorillonite as a function of pH and ionic strength in equilibrium with atmospheric pCO_2 and in carbonate free conditions. They suggested the formation of uranyl carbonate surface complexes based on the identification by EXAFS of one C shell around 2.9 Å.

Despite the existing studies, there is still a considerable gap in our atomistic level understanding of uranyl adsorption onto clay mineral surfaces from aqueous solution, particularly in the presence of carbonate. Coupling macroscopic and spectroscopic measurements enhances the credibility of the results and reduces uncertainties. The present study deals with the sorption of uranyl on montmorillonite under various conditions (pH, U(VI) concentration, presence and absence of carbonate) by combining different approaches i.e. macroscopic sorption experiments, surface complexation modelling and EXAFS measurements.

2. MATERIALS AND METHODS

2.1. Materials

Supra-pure grade chemicals and ultra pure de-ionised water were used to prepare all the solutions. SWy-1 montmorillonite obtained from the Source Clay Repository of the Clay Minerals Society was taken for the sample preparation after conversion into the Na-form. A purifying procedure was applied to the "as received" clay powder to obtain, as far as possible, a single phased suspension of Na-montmorillonite in a 1:1 background electrolyte. This procedure has been described previously by Baeyens and Bradbury (1995a), and only an outline will be given here.

SWy-1 montmorillonite was washed three times with 1 M $NaClO_4$ to remove all soluble salts and/or sparingly soluble minerals such as calcite and to convert the clay into the homo-ionic Na-form. Separation of the <0.5 μm Na-SWy-1 fraction was achieved through peptisation by successive washing with de-ionised water, pre-equilibrated with a small quantity of montmorillonite, combined with centrifugation (~7 min at ~600*g* (max.)), decantation of the supernatant solution, and subsequent flocculation with 1 M $NaClO_4$. Soluble hydroxy-aluminium compounds were removed by an acid treatment (pH 3.5, 1 h) followed by phase separation and neutralisation with 1 M $NaClO_4$ (pH 7). Clay batches for the sorption experiments were prepared in 0.1 M $NaClO_4$ from the stock suspension by the dialysis technique. The clay content in the final suspensions was determined by heating weighed aliquots to constant weight at 105 °C and correcting for the salt content. The cation exchange capacity, CEC, determined using the

Table 1
Summary of the experimental conditions for the U(VI) sorption edges and isotherms on Na-SWy-1 in 0.1 M $NaClO_4$.

Experimental conditions	U(VI) sorption edges			U(VI) sorption isotherms	
	No carbonate	Atmospheric pCO_2	1, 3 and 5 mM $NaHCO_3$	No carbonate	Atmospheric pCO_2
pH Range	2.7–9.5	4–10	7–9.2	~8	~8
Buffers	Yes	No	Yes	Yes	No
S:L ratio (g L^{-1})	0.9	2.5	4.3	1	1.5 and 2
Initial U conc. (M)	9×10^{-8}	9×10^{-8}	9×10^{-8}	5×10^{-8}–10^{-4}	5×10^{-8}–2.5×10^{-4}
Equilibration (days)	7	7	7	7	7

^{134}Cs isotopic dilution method (Baeyens and Bradbury, 2004) was measured to be 0.85 eq kg^{-1}, which is in a good agreement with the value of 0.87 eq kg^{-1} given by Baeyens and Bradbury (1997) for Na-SWy-1 montmorillonite.

2.2. Batch sorption measurements on Na-SWy-1

Batch sorption experiments were carried out on conditioned and purified Na-SWy-1 montmorillonite in the absence and presence of carbonate to produce two main types of data sets: sorption measured at trace U(VI) concentration as a function of pH at fixed ionic strength (*sorption edges*), and sorption measured as a function of U(VI) concentration at constant pH and ionic strength (*sorption isotherms*). Both types of data sets are necessary for the modelling procedure to derive strong and weak site surface binding constants for U(VI) on montmorillonite.

Carbonate free sorption experiments were performed in a glove box under N_2-atmosphere ($O_2 < 3$ ppm). Experiments in the presence of carbonate were carried out under atmospheric conditions ($pCO_2 = 10^{-3.5}$ bar) and in closed systems (at higher pCO_2). The experimental conditions are summarized in Table 1.

Sorption edge measurements at $^{233}U(VI)$ trace concentration ($C_{initial}$ ~9×10^{-8} M) as a function of pH in 0.1 M $NaClO_4$ were carried out at solid to liquid (S:L) ratios between 0.9 and 4.3 g L^{-1} in 40 ml centrifuges tubes. In the presence of carbonate, sorption edges were measured: (i) in equilibrium with the atmospheric $pCO_2 = 10^{-3.5}$ bar and (ii) at variable pCO_2 *i.e.* in the presence of 1, 3 and 5 mM $NaHCO_3$. The latter experiments are not in equilibrium with the air atmosphere and were carried out in a closed system. In both cases, the total carbonate concentration was adjusted as a function of pH using $NaHCO_3/Na_2CO_3$ solutions. The appropriate concentrations of carbonate and bicarbonate necessary to reproduce atmospheric pCO_2 conditions were calculated theoretically for each pH value. The pH values of the carbonate free experiments, and, the experiments in 1, 3 and 5 mM $NaHCO_3$, were buffered with different buffers *i.e.* $CH_3COONa{\cdot}3H_2O$ (sodium acetate), $C_6H_{13}NO_4S$ (MES), $C_7H_{15}NO_4S$ (MOPS), $H_2NC(CH_2OH)_3$ (TRIS) or $C_8H_{17}NO_3S$ (CHES) (BioChemika MicroSelect, Fluka) at concentrations of 2×10^{-3} M to prevent pH drift. These buffers were chosen because of their very weak tendencies to complex with metal ions (Perrin and Dempsey, 1974). Experimental tests carried out on conditioned Na-SWy-1 demonstrated that the buffers (at concentrations of 2×10^{-3} M) did not have any significant effect on sorption (Baeyens and Bradbury, 1995b).

After labelling with ^{233}U and shaking end-over-end for 7 days, the suspensions were centrifuged at 105,000*g* (max) for 1 h using a Beckman Coulter Avanti™ J30I High-Performance Centrifuge. Carbonate free samples were returned to the glove box for sampling of the supernatant and pH measurements, whereas the samples in the presence of carbonate were measured under atmospheric conditions. The pH of each sample was measured using a Metrohm combined electrode. The electrode was calibrated with Merck buffers. All experiments were carried out in triplicate. Radiochemical assays of ^{233}U in the supernatants were performed using a Packard Tri-Carb Alpha/Beta liquid scintillation counter together with standard labelled solutions.

For the sorption isotherm determinations, a series of stable $UO_2(NO_3)_2$ solutions covering the U(VI) concentration range required, was prepared at pH 8 in 0.1 M $NaClO_4$ background electrolyte containing 2×10^{-3} M TRIS buffer and labelled with ^{233}U. A similar experimental procedure to that described above was then followed. The measurements were either carried out in a glove box (absence of CO_2) or in equilibrium with atmospheric pCO_2 (Table 1).

The results of the batch sorption experiments are expressed in terms of the logarithm of the solid liquid distribution ratio, R_d, defined in the customary manner as:

$$R_d = \frac{(C_{init} - C_{eq})}{C_{eq}} \cdot \frac{V}{m}$$

where C_{init}: initial aqueous concentration of U(VI) (M), C_{eq}: equilibrium aqueous concentration of U(VI) (M), V: volume of liquid phase (L), m: mass of solid phase (kg).

2.3. Two Site Protolysis Non-Electrostatic Surface Complexation and Cation Exchange (2SPNE SC/CE) model

The 2SPNE SC/CE model (Bradbury and Baeyens, 1997) was used to describe quantitatively the sorption data obtained in this work. This non-electrostatic, quasi-mechanistic thermodynamic sorption model calculates the uptake of aqueous metal species by a combination of cation exchange and pH dependent inner-sphere surface complexation at the amphoteric edge sites (Sposito, 1984). The 2SPNE SC/CE sorption model, and the modelling procedure, have been described in detail on many occasions and will not be further addressed here.

Table 2
Summary of the non-adjustable parameters determined for Na-SWy-1 montmorillonite (Bradbury and Baeyens, 1997): cation exchange capacity (CEC), surface hydroxyl group capacities and protolysis constants.

Site types	Site capacities
$\equiv S^{S}OH$	2.0×10^{-3} mol kg^{-1}
$\equiv S^{W1,W2}OH$	4.0×10^{-2} mol kg^{-1}
CEC	8.7×10^{-1} eq kg^{-1}
Protolysis reactions	**log $K_{protolysis}$**
$\equiv S^{S,W1}OH + H^+ \Leftrightarrow \equiv S^{S,W1}OH_2^+$	4.5
$\equiv S^{S,W1}OH \Leftrightarrow \equiv S^{S,W1}O^- + H^+$	−7.9
$\equiv S^{W2}OH + H^+ \Leftrightarrow \equiv S^{W2}OH_2^+$	6.0
$\equiv S^{W2}OH \Leftrightarrow \equiv S^{W2}O^- + H^+$	−10.5

The sorption of U(VI) on Na-SWy-1 was modelled using the non-adjustable parameters for montmorillonite given in Table 2 and the hydrolysis and carbonate complexation constants taken from the uranium NEA Chemical Thermodynamic Database (Guillaumont et al., 2003), Table 3.

Thermodynamic calculations (aqueous speciation and the modelling of the sorption data) were performed with the code MINSORB (Bradbury and Baeyens, 1997). MINSORB is derived from geochemical code MINEQL (Westall et al., 1976) and contains subroutines for calculating cation exchange and surface complexation reactions simultaneously.

2.4. Sample preparation for EXAFS measurements

Samples for the EXAFS investigations were prepared in a batch mode in 200 ml polypropylene vessels in a similar way to that described in Section 2.2, but in the absence of the ^{233}U tracer. One carbonate free sample (U_Mont1: under N_2-atmosphere) and two carbonate containing samples (U_Mont2: atmosphere equilibrated; and U_Mont3: in 1 mM $NaHCO_3$) were prepared at pH ~8 in the presence of the pH buffer TRIS. The three samples had similar U(VI) loadings. These loadings were determined by taking 40 ml aliquots of each clay suspension, centrifuging for 1 h at 105,000*g* (max) and then analyzing the supernatant for U by ICP-OES to determine the U(VI) equilibrium concentrations. The experimental conditions used for the preparation of the samples are summarized in Table 4.

In order to improve the sensitivity of the EXAFS measurements, the U(VI) montmorillonite samples were prepared as highly textured self-supporting dry montmorillonite films (Manceau et al., 1998). After a reaction time of 14 days, 40 mL of each suspension was slowly filtrated through a 47 mm diameter filter with a 0.47 μm pore size (Millipore) to produce three oriented self-supporting films. The filtrations were performed in a closed vessel. Additionally, the filtration of the carbonate free sample was carried out under a continuous flow of N_2 to avoid contamination

Table 3
Aqueous uranyl hydrolysis and carbonate complexation constants used in the modelling (Guillaumont et al., 2003).

	log K
Aqueous U(VI) hydrolysis reactions	
$UO_2^{2+} + H_2O \Leftrightarrow UO_2(OH)^+ + H^+$	−5.25
$UO_2^{2+} + 2H_2O \iff UO_2(OH)_2^0 + 2H^+$	−12.15
$UO_2^{2+} + 3H_2O \iff UO_2(OH)_3^- + 3H^+$	−20.25
$UO_2^{2+} + 4H_2O \iff UO_2(OH)_4^{2-} + 4H^+$	−32.40
Aqueous U(VI) carbonate reactions	
$UO_2^{2+} + CO_3^{2-} \iff UO_2CO_3^0$	9.94
$UO_2^{2+} + 2CO_3^{2-} \iff UO_2(CO_3)_2^{2-}$	16.61
$UO_2^{2+} + 3CO_3^{2-} \iff UO_2(CO_3)_3^{4-}$	21.84
$2UO_2^{2+} + CO_3^{2-} + 3H_2O \iff (UO_2)_2CO_3(OH)_3^{3-}$	−0.86
$3UO_2^{2+} + CO_3^{2-} + 3H_2O \iff (UO_2)_2CO_3(OH)_3^{3-}$	0.66
$3UO_2^{2+} + 6CO_3^{2-} \iff (UO_2)_3(CO_3)_6^{6-}$	54.0

Table 4
EXAFS samples description: S:L ratio = 2 g L^{-1}, background electrolyte 0.1 M $NaClO_4$, pH ~8.

Sample	$NaHCO_3$ (mM)	pH	pCO_2 (bar)	U_{eq} conc. (M)	U loading (mmol kg^{-1})	log R_d (L kg^{-1})
U_Mont1	None	7.98	$<10^{-5.5}$	6.72×10^{-7}	7.0	4.02
U_Mont2	0.61	7.98	$10^{-3.5}$	5.86×10^{-6}	6.9	3.08
U_Mont3	1.0	7.95	$10^{-3.3}$	9.84×10^{-6}	4.9	2.71

by atmospheric carbonate and was returned to the glove box for drying. The dried clay films were cut into eight slices and stacked on a Plexiglas sample holder to obtain samples thick enough for the EXAFS measurements in fluorescence mode.

2.5. EXAFS Data Acquisition and Analysis

Uranium L_{III}-edge EXAFS spectra were recorded in fluorescence mode at the Rossendorf Beamline (ROBL) at the European Synchrotron Radiation Facility (ESRF) in Grenoble, France, using a Si(1 1 1) double-crystal monochromator.

Self-supporting montmorillonite films were mounted on a goniometer and the EXAFS spectra were recorded at an angle of 35° between the clay film (*i.e.* phyllosilicate basal plane) and the electric field vector E of the linear polarized X-ray beam. At this particular angle, the powder and polarized spectra are identical (Manceau et al., 1998). Polarized-EXAFS (P-EXAFS) measurements were carried out only on the carbonate free sample U_Mont1 (Table 2) at angles of 10°, 35°, and 55°. The angle at 80° could not be measured. The application of P-EXAFS on highly oriented self-supporting montmorillonite films allows the contribution of cations from silicium tetrahedral sheets to be minimized by orienting the film plane parallel to the polarization direction of the X-ray beam, and, conversely, the contribution of the cations from the aluminium octahedral sheets to be extinguished in the perpendicular orientation to the polarization direction (Manceau et al., 1998).

The fluorescence spectra were collected at room temperature with a 13-element, high-purity Germanium solid-state detector. The first inflection point of the absorption spectrum of an yttrium foil (17,038 eV), which was measured simultaneously in transmission mode, was used for energy calibration. Several EXAFS scans were collected from each of the U loaded clay samples and averaged to improve the signal to noise ratio (typically ~10 scans).

EXAFS data reduction and fitting was performed using the Athena–Artemis-IFEFFIT package (Newville et al., 1993; Newville, 2001; Ravel and Newville, 2005) following standard procedures (Stern, 1988). The $\chi(k)$ function was extracted from the raw data by fitting a linear function to the pre-edge region and a spline function to the post-edge region. The resulting EXAFS $\chi(k)$ spectrum was weighted by k raised to the power of 3 to compensate for the dampening of the EXAFS amplitude with increasing k. Fourier transforms (FTs) were obtained from $k^3\chi(k)$ functions (typical range 3.6–13.6 $Å^{-1}$) using a Kaiser-Bessel window (with dk = 1 $Å^{-1}$).

Theoretical backscattering phase and amplitude functions for the paths U–O_{ax}, U–O_{eq}, U–Si_1, U–Si_2, U–C, U–O_{dist} and U–Fe used for the fitting of the spectra, were generated from the crystal structure of soddyite $(UO_2)_2SiO_4{\cdot}2H_2O$ (Demartin et al., 1992), rutherfordine UO_2CO_3 (Finch et al., 1999) and uranium iron oxide $UFeO_4$ (Bacmann and Bertaut, 1967), using FEFF 8.0 (Rehr et al., 1991; Ankudinov et al., 1998). The initial fitting was performed through selection of single scattering paths found to contribute significantly to the spectra.

Structural parameters were obtained by fitting the experimental data with several coordination shells. For the multi-shell fitting in R-space, the k-range started always at 3.6 $Å^{-1}$. The value of k_{max} for the FT of each sample was dependent on the quality of the experimental spectra (Tables 7 and EA3 (Electronic annex)). The FT peaks of interest were selected and fitted in the R-space in the range 0.5–3.7 Å. The number of variable parameters during the fitting process was always less than the number of independent points (Nyquist theorem), as defined in IFEFFIT (Stern, 1993).

The amplitude reduction factor, S_0^2, was set equal to 1.0 (Hennig et al., 2002). A global threshold energy, ΔE_0, was allowed to vary during the fit but was linked for all paths.

Most of the fitting parameters (bond distances, R, coordination number, CN and Debye–Waller factors, σ^2) were allowed to adjust freely except for the Debye–Waller parameters σ^2 of U–Si_1, U–Si_2 and U–Fe shells; these were fixed in all the samples to avoid strong correlations and are given in Table 7. All the samples showed a splitted equatorial oxygen shell U-O_{eq1} and U-O_{eq2}, and the values of the σ^2 for both shells were linked. The multiple scattering (MS) path of the uranyl moiety was linked to the U–O_{ax} scattering parameters by constraining its fit parameters to values of the U–O_{ax} single scattering (SS), as described in Hudson et al. (1996). The quality of the fit was quantified by both, the *R-factor* (R_f) and *reduced* χ^2 as used by FEFFIT (See Electronic annex EA1).

The polarized spectra of the sample U_Mont1 were fit together using common values for ΔE_0, EXAFS distances, and Debye–Waller parameters of the j^{th} shell (Schlegel et al., 2001; Vespa et al., 2010). The numbers of neighboring atoms (N^{α}) were fit independently for each α angle.

3. SORPTION RESULTS AND MODELLING

3.1. U(VI) sorption on Na-SWy-1 montmorillonite in the absence of carbonate

3.1.1. Experimental data and modelling

Fig. 1a shows the uptake of U(VI) at trace concentration as a function of pH on Na-SWy-1 montmorillonite. The sorption of U(VI) increases as a function of pH reaching a maximum at pH ~6 ($\log R_d = 5.4 \pm 0.2$ L kg^{-1}), whereafter the sorption decreases slightly to $\log R_d = 4.4 \pm 0.2$ L kg^{-1} at pH 9.4. The data measured by Bradbury and Baeyens (2005) have been included in this figure (open symbols) and agree well with the new measurements.

The U(VI) sorption isotherm measured on Na-SWy-1 at pH ~8 in 0.1 M $NaClO_4$ together with sorption isotherms obtained at pH 5 and 6.8 by Bradbury and Baeyens (2005) are presented in the Fig. 1b–d. The sorption of U(VI) on montmorillonite shows a non-linear behaviour at the three different pH values.

Both types of data sets, sorption edge and isotherms were modelled using the aqueous uranyl hydrolysis constants given in Table 3, which were different from the hydrolysis data used in Bradbury and Baeyens (2005) and hence the surface complexation (SC) constant are also different.

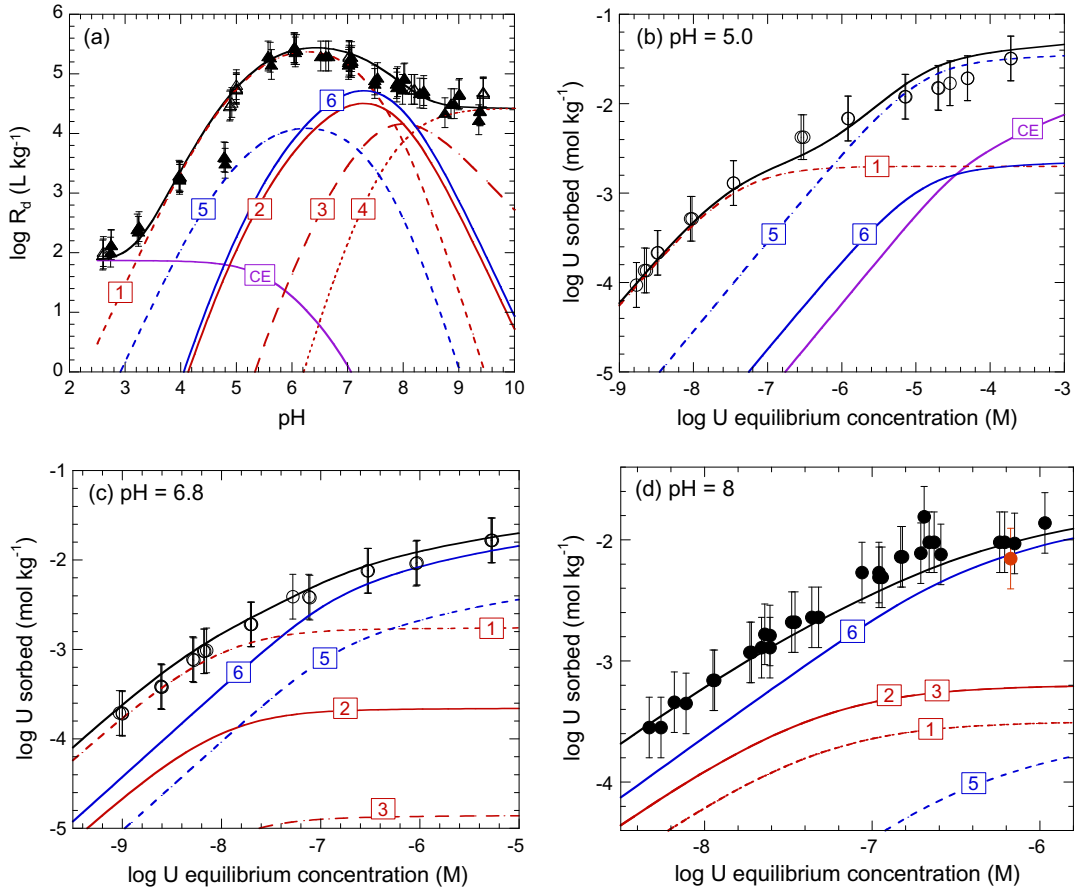

Fig. 1. U(VI) sorption on Na-SWy-1 in 0.1 M $NaClO_4$. (a) Sorption edge measurements (▲) this study; (△) from Bradbury and Baeyens (2005). Sorption isotherms (b) at pH 5, (c) pH 6.8 from Bradbury and Baeyens (2005), (d) at pH 8, this study. Continuous black curves are the best fits obtained with the 2SPNE SC/CE sorption model (see text for details). Curves labelled (1–6) and CE represent the contribution to the overall sorption of the major individual U(VI) surface species in the absence of carbonate (see Table 5). (●) EXAFS sample: U_Mont1.

The only adjustable parameters available for fitting the sorption data are the stability constants for the surface complexation reactions. A stepwise modelling procedure was carried out in which the edge data was modelled first followed by the isotherm data sets. At low pH (Fig. 1a) the uptake is interpreted in terms of cation exchange (CE) on the permanently charged planar sites arising from isomorphous substitutions in the montmorillonite lattice. The UO_2^{2+}-Na^+ exchange is described by the CE reaction given in Table 5. The pH dependent sorption behaviour is modelled in terms of SC reactions at the amphoteric surface hydroxyl groups (≡SOH sites) situated at the montmoril-

Table 5
Summary of the surface complexation constants and selectivity coefficients characterizing the sorption of U(VI) on Na-SWy-1 in the absence of carbonate.

Surface complexation reactions	$\log^{S,W}K$
Strong sites	
(1) $\equiv S^SOH + UO_2^{2+} \Leftrightarrow \equiv S^SOUO_2^+ + H^+$	3.1
(2) $\equiv S^SOH + UO_2^{2+} + H_2O \Leftrightarrow \equiv S^SOUO_2OH^0 + 2H^+$	−4.6
(3) $\equiv S^SOH + UO_2^{2+} + 2H_2O \Leftrightarrow \equiv S^SOUO_2(OH)_2^- + 3H^+$	−12.6
(4) $\equiv S^SOH + UO_2^{2+} + 3H_2O \Leftrightarrow \equiv S^SOUO_2(OH)_3^{2-} + 4H^+$	−20.9
Weak sites	
(5) $\equiv S^{W1}OH + UO_2^{2+} \Leftrightarrow \equiv S^{W1}OUO_2^+ + H^+$	0.5
(6) $\equiv S^{W1}OH + UO_2^{2+} + H_2O \Leftrightarrow \equiv S^{W1}OUO_2OH^0 + 2H^+$	−5.7
Cation exchange reaction	log K_c
CE: $2Na^+$-clay + $UO_2^{2+} \Leftrightarrow UO_2^{2+}$-clay + $2Na^+$	0.45

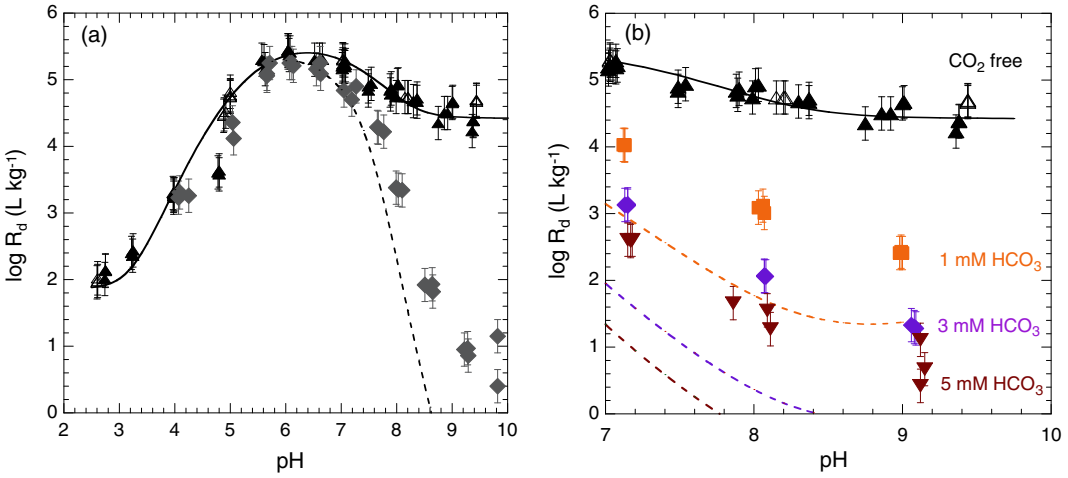

Fig. 2. U(VI) sorption edge measurements on Na-SWy-1 in the absence of carbonate (▲, △) and (a) in equilibrium with atmospheric pCO_2 (◆); (b) in the presence of 1, 3 and 5 mM $NaHCO_3$. Dashed lines: modelled curves assuming that U(VI) carbonate complexes do not sorb.

lonite clay platelet edges. The pH dependent sorption data was modelled with a series of four surface complexation reactions (Eqs. (1)–(4) in Table 5) on the strong sites ($\equiv S^SOH$) of montmorillonite.

In order to ensure any credibility to surface complexation modelling, more than one set of experimental data should be reproducible with the same set of surface complexation reactions and constants. The sorption isotherms at pH 5, 6.8 and 8 given in Fig. 1b, c and d, respectively, were modelled. Two additional surface complexation reactions on the weak sites ($\equiv S^{W1}OH$) were required. With the surface complexation constants obtained on the weak sites the sorption edge at trace concentration (Fig. 1a) was refitted. This procedure was repeated until all data sets were successfully modelled with the same set of parameters. The results are summarized in Table 5 including all surface complexation reactions and associated constants on strong and weak sites. In Fig. 1 the contribution of the different surface species for each data set is indicated by the colored curves. It should be noted that at pH ~8 even at low U(VI) equilibrium concentration sorption on weak sites is taking place and $\equiv S^{W1}OUO_2OH^0$ is the dominating surface species (see Fig. 1a and d).

3.2. U(VI) sorption on Na-SWy-1 in the presence of carbonate

3.2.1. Sorption edge data

The uptake of U(VI) at trace concentration as a function of pH on Na-SWy-1 in equilibrium with atmospheric pCO_2, and in the presence of 1, 3 and 5 mM $NaHCO_3$, are shown in Fig. 2a and b, respectively.

In the sorption experiments at a constant pCO_2 of $10^{-3.5}$ bar (Fig. 2a), no influence of carbonate is observed up to pH ~6.5. The log R_d values are close to those measured in the carbonate-free system. However, at pH values greater than 6.5, a pronounced decrease in the U(VI) sorption is observed with increasing pH and carbonate concentration. The log R_d decreases down to values below 1 L kg^{-1} at pH 9.

At higher carbonate levels, in the pH range 7–8, Fig. 2b, the effect on U(VI) sorption is even more significant. In the presence of 1 mM $NaHCO_3$, the log R_d decreases to ~3.1 ± 0.2 L kg^{-1} at pH ~8. At the highest carbonate concentration, 5 mM $NaHCO_3$, the log R_d decreases to ~1.3 ± 0.5 L kg^{-1} at pH ~8.1.

3.2.2. Modelling sorption edge data

In a first modelling approach the sorption parameters derived in Section 3.1 were applied to the data under the assumption that no additional U(VI) surface complexation reactions are taking place *i.e.* aqueous U(VI) carbonate complexes were treated as being non-sorbing. The results of this modelling approach are presented as dashed lines in Fig. 2a and b. The aqueous uranyl carbonate complexation constants used in the modelling are given in Section 2.3, Table 3. Under the given experimental conditions *i.e.* at trace U(VI) concentrations, only the mononuclear uranyl carbonate complexes are important.

Clearly, Fig. 2 illustrates that in all cases the model predictions failed to reproduce the experimental data sets above pH ~7, and largely underestimate the experimental data at high carbonate concentrations (Fig. 2b). The calculated effect of the influence of carbonate on the sorption of U(VI) is greater than experimentally observed (up to two orders of magnitude). The precipitation of any solid uranyl phase leading to an increased uptake can be excluded at the U(VI) concentration used in the experiments (~9×10^{-8} M).

There are two possible explanations for these discrepancies. Firstly, the aqueous thermodynamic complexation data of the uranyl carbonate complexes given in Table 3 are too strong. However, this assumption seems rather unrealistic because the selected NEA data have a very high degree of reliability. The second possibility is that uranyl carbonate surface complexes are forming on the clay surface. Both possibilities are examined below.

3.2.2.1. Uranyl sorption modelling with modified aqueous thermodynamic data. The dotted curve in Fig. 3a presents

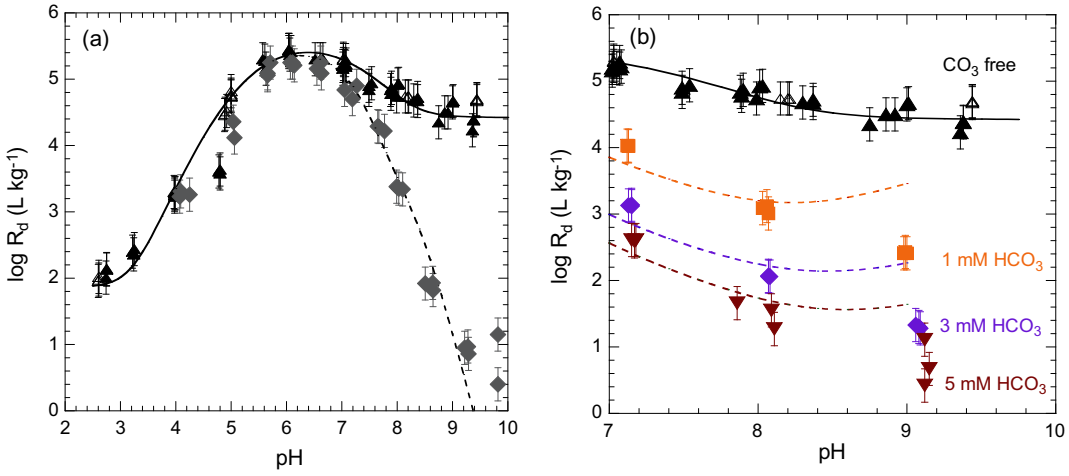

Fig. 3. U(VI) sorption edge measurements on Na-SWy-1 in the absence of carbonate (▲, △) and (a) in equilibrium with atmospheric pCO_2 (◆); (b) in the presence of 1, 3 and 5 mM $NaHCO_3$. Dashed lines: modelled curves with modified stability constants for aqueous U(VI) carbonate complexes.

Table 6
Surface complexation constants on strong sites ($\log^{S}K$) and weak sites ($\log^{W1}K$) for U(VI)-carbonate complexes on Na-SWy-1 montmorillonite.

Surface complexation reaction	$\log^{S,W1}K$
(7) $\equiv S^{S}OH + UO_2^{2+} + CO_3^{2-} \Leftrightarrow \equiv S^{S}OUO_2CO_3^{-} + H^{+}$	9.8
(8) $\equiv S^{S}OH + UO_2^{2+} + 2CO_3^{2-} \Leftrightarrow \equiv S^{S}OUO_2(CO_3)_2^{3-} + H^{+}$	15.5
(9) $\equiv S^{W1}OH + UO_2^{2+} + CO_3^{2-} \Leftrightarrow \equiv S^{W1}OUO_2CO_3^{-} + H^{+}$	9.3

the best fit to the experimental data measured in equilibrium with atmospheric pCO_2. The modified uranyl carbonate complexation constant used to achieve this fit were $\log K_1(UO_2CO_3^0) = 9.4$; $\log K_2(UO_2(CO_3)_2^{2-}) = 16.1$; $\log K_3(UO_2(CO_3)_3^{4-}) = 19.4$. The constants for the first two complexes had to be lowered by approximately 0.5 log units whereas the third complex had to be reduced by more than 2 orders of magnitude (see Table 3). The next step was to see how well these modified uranyl carbonate constants could be used to describe the sorption data sets obtained at fixed carbonate contents. The results are presented in Fig. 3b. The calculated curves fit the measurements at pH 7 and 8 reasonably well but totally fail to describe the sorption data at pH 9. Based on this observa-

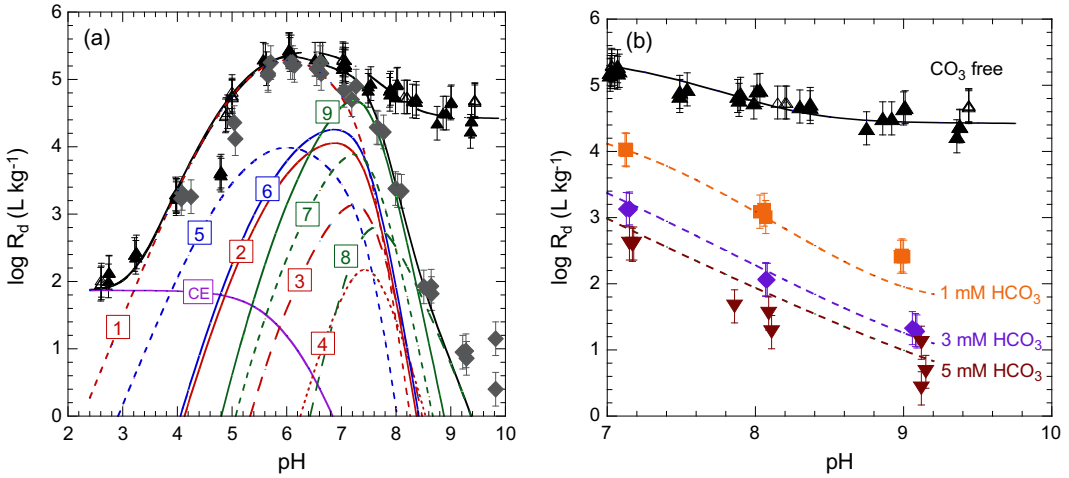

Fig. 4. U(VI) sorption edge measurements on Na-SWy-1in the absence of carbonate (▲, △) and (a) in equilibrium with atmospheric pCO_2 (◆); (b) in 1, 3 and 5 mM $NaHCO_3$. The modelled curves include ternary uranyl surface complexes on the strong sites: $\equiv S^{S}OUO_2CO_3^{-}$ and $\equiv S^{S}OUO_2(CO_3)_2^{3-}$ and one on the weak sites: $\equiv S^{W1}OUO_2CO_3^{-}$. Curves labelled (1–9) and CE represent the contribution to the overall sorption of the major individual U(VI) surface species (see Table 5 and 6).

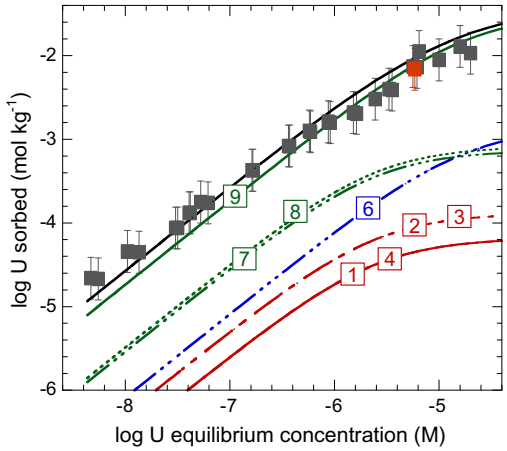

Fig. 5. U(VI) sorption isotherm on Na-SWy-1 measured in equilibrium with atmospheric pCO_2 at pH 8 (■). Continuous black curves are the best fits obtained with the 2SPNE SC/CE sorption model (see text for details). Curves labelled (1–9) represent the contribution to the overall sorption of the major individual U(VI) surface species (see Table 5 and 6). (■) EXAFS sample U_Mont2.

tion the hypothesis that the aqueous uranyl carbonate stability constants are too strong seems highly unlikely.

3.2.2.2. Uranyl sorption modelling assuming the formation of ternary uranyl carbonate surface complexes. A stepwise approach was adopted to model the sorption data obtained in the presence of carbonate by considering, in sequence, simple chemically reasonable surface complexation reactions involving U(VI) carbonate complexes. An iterative modelling procedure similar to the one described in Section 3.1.1 was applied (modelling of sorption edge and isotherm are linked) to derive the surface complexation constants. The calculated aqueous speciation for U(VI) under the appropriate experimental conditions was used to guide the choice of the potential surface complexes. Aqueous speciation calculations indicated that the U(VI)-mono and di-carbonate complexes were the dominant aqueous species. All of the experimental sorption edges measured in the presence of carbonate could be quantitatively modelled by including two additional U(VI)-carbonate surface complexes on the strong sites and one on the weak sites. The latter results from the iterative modelling procedure including the sorption isotherm (see Section 3.2.3). The surface complexation reactions and their associated stability constants, are summarized in Table 6. The modelling results are presented in Fig. 4a and b.

The results show that for the four independent experimental data sets available (atmospheric pCO_2, in 1, 3 and 5 mM $NaHCO_3$) a consistent picture is obtained, and only slight deviations from the experimental data are observed. The results of this modelling approach strongly suggest that uranyl carbonate complexes do exist at the clay edge surfaces.

3.2.3. Sorption isotherm data and modelling

Fig. 5 shows the U(VI) sorption isotherm measured on conditioned Na-SWy-1 at pH ~8 in equilibrium with atmospheric pCO_2. At an equilibrium concentration of 10^{-8} M, the amount of U(VI) sorbed is more than a order of magnitude lower compared to the isotherm in the absence of

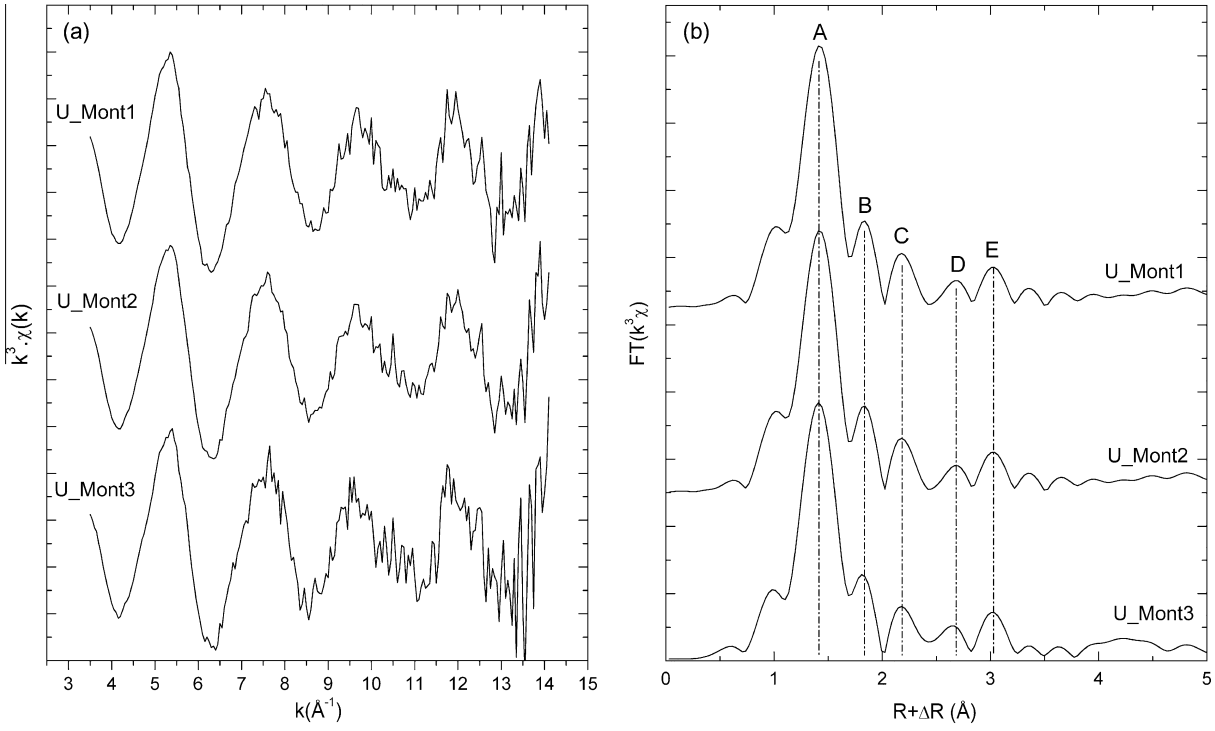

Fig. 6. (a) Experimental k^3-weighted χ functions and (b) the corresponding experimental RSFs obtained for the U(VI) montmorillonite samples U_Mont1, U_Mont2 and U_Mont3 at 35°. (A–E) indicate different backscattering contributions.

Table 7
Structural parameters for the samples U_Mont1, U_Mont2 and U_Mont3 derived from the EXAFS analysis considering a) two Si/Al shells and b) one Si/Al shell and one Fe shell. FT range from 3.6 to 13.6 $Å^{-1}$ and FT^{-1} from 1 to 4 Å.

Sample		Shell	CN	R (Å)	σ^2 [$Å^2$]	ΔE_0[d] [eV]	R_f Red-χ^2	N_{idp} N_{var}
U_Mont1	(a)	U–O_{ax}	2.2(2)	1.80(1)	0.0029(8)	9.8	10^{-4}	17
		U–O_{eq1}	3.1(3)[a]	2.30(2)	0.007(2)[b]		3.1	12
		U–O_{eq2}	2.9(3)[a]	2.48(2)	0.007(2)[b]			
		U–Al_1/Si_1	0.9(3)	3.09(2)	0.003[c]			
		U–Al_2/Si_2	0.9(4)	3.28(3)	0.003[c]			
	(b)	U–O_{ax}	2.2(3)	1.80(1)	0.003(1)	9.1	1.6×10^{-4}	17
		U–O_{eq1}	3.2(3)[a]	2.29(2)	0.007(2)[b]		4.7	12
		U–O_{eq2}	2.8(3)[a]	2.48(3)	0.007(2)[b]			
		U–Al_1/Si_1	0.5(3)	3.07(3)	0.003[c]			
		U–Fe	0.3(2)	3.42(3)	0.003[c]			
U_Mont2	(a)	U–O_{ax}	2.1(2)	1.80(1)	0.003(1)	9.8	10^{-4}	17
		U–O_{eq1}	3.2(3)[a]	2.29(2)	0.006(2)[b]		4.1	12
		U–O_{eq2}	2.8(3)[a]	2.49(2)	0.006(2)[b]			
		U–Al_1/Si_1	0.9(3)	3.10(2)	0.003[c]			
		U–Al_2/Si_2	0.9(4)	3.29(3)	0.003[c]			
	(b)	U–O_{ax}	2.1(3)	1.80(1)	0.002(1)	9.1	1.8×10^{-4}	17
		U–O_{eq1}	3.3(3)[a]	2.29(2)	0.007(1)[b]		6.3	12
		U–O_{eq2}	2.7(3)[a]	2.49(2)	0.007(1)[b]			
		U–Al_1/Si_1	0.6(3)	3.08(3)	0.003[c]			
		U–Fe	0.3(2)	3.43(4)	0.003[c]			
U_Mont3	(a)	U–O_{ax}	2.1(2)	1.80(1)	0.0027(6)	9.1	9.3×10^{-5}	17
		U–O_{eq1}	3.3(2)[a]	2.29(2)	0.006(1)[b]		0.8	12
		U–O_{eq2}	2.7(1)[a]	2.49(2)	0.006(1)[b]			
		U–Al_1/Si_1	1.3(3)	3.09(2)	0.003[c]			
		U–Al_2/Si_2	1.2(4)	3.28(2)	0.003[c]			
	(b)	U–O_{ax}	2.1(3)	1.80(1)	0.0026(6)	7.8	1.6×10^{-4}	17
		U–O_{eq1}	3.5(3)[a]	2.28(2)	0.007(1)[b]		1.4	12
		U–O_{eq2}	2.5(1)[a]	2.48(2)	0.007(1)[b]			
		U–Al_1/Si_1	0.8(3)	3.08(2)	0.003[c]			
		U–Fe	0.5(2)	3.42(2)	0.003[c]			

Note: CN: coordination number; R: distance; σ^2: Debye–Waller factor; R_f and Red-χ^2: quality of fit as defined in the electronic annex; N_{idp}: number of independent parameters; N_{var}: number of variable parameters; number in parentheses represent the errors in the last digit.
[a] The sum of the CN of equatorial oxygens was constrained to 6.
[b] Values coupled during the fit.
[c] Value fixed during the fit.
[d] E_0 value was allowed to vary but linked for all paths.

carbonate (see Fig. 1d). At higher U(VI) equilibrium concentrations the sorption remains lower but the difference is less pronounced.

The same modelling procedure described for the carbonate free isotherm (Section 3.1.1) was used to model the U(VI) isotherm obtained in the presence of carbonate. In a first step the SC constants on the strong sites and the weak sites derived in the absence of carbonate (Table 5), and the SC constants of the ternary carbonate surface complexes on strong sites ($\equiv S^SOUO_2CO_3^-$ and $\equiv S^SOUO_2(CO_3)_2^{3-}$) (Table 6) were used. The best fit to the experimental was obtained by including one additional ternary uranyl-carbonate surface complex ($\equiv S^{W1}OUO_2CO_3^-$) on the weak sites (Table 6).

The inclusion of ternary uranyl-carbonate complexes on the strong and weak sites in the sorption modelling allowed the uptake of U(VI) on Na-SWy-1 to be quantitatively described under a wide range of conditions (U(VI) concentration, pH, pCO_2).

4. EXAFS MEASUREMENTS

4.1. EXAFS of U(VI) sorbed on Na-SWy-1 in the absence and presence of carbonate

EXAFS measurements were carried out on three U(VI) loaded montmorillonite samples prepared in the absence (U_Mont1) and in the presence of carbonate (U-Mont2 and U_Mont3). All samples were prepared at pH 8 and have similar U(VI) loadings, see Table 4. The U(VI) loadings for U_Mont1 and U_Mont2 at the measured U(VI) equilibrium concentration are in a very good agreement

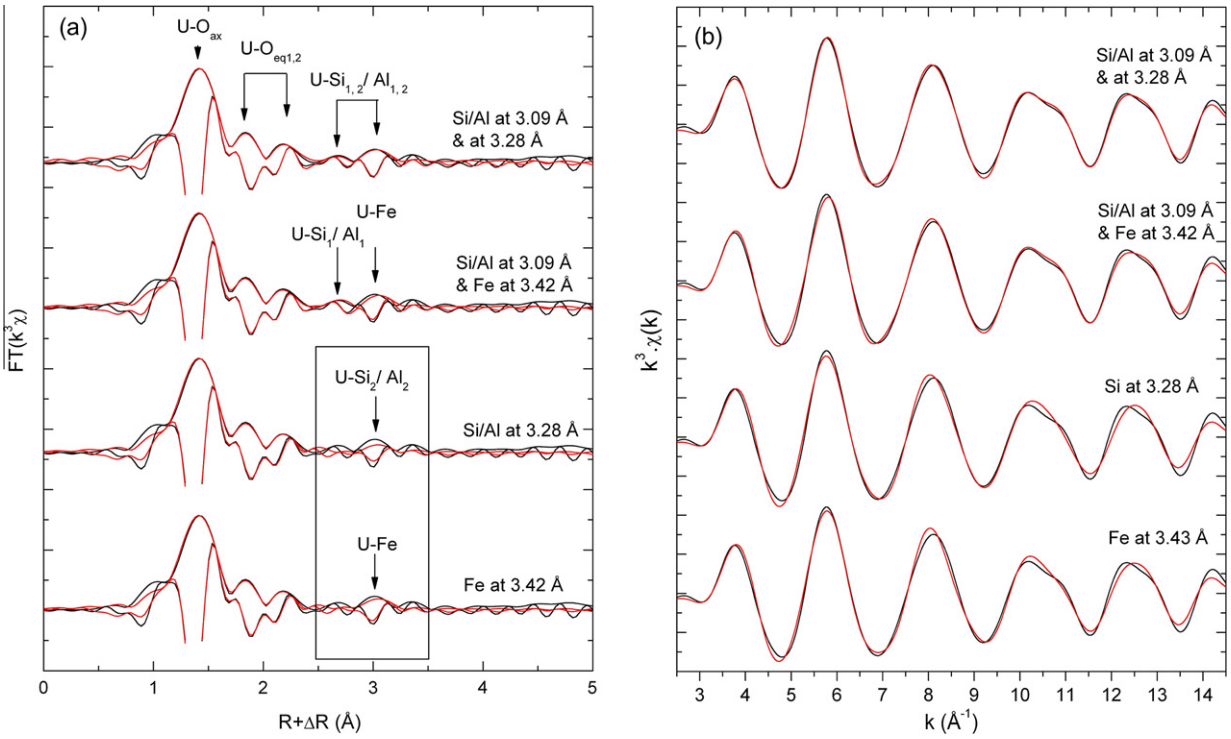

Fig. 7. (a) FTs (moduli and imaginary parts) of experimental EXAFS spectra measured at 35° for the sample U_Mont1 (black lines) and the fits obtained considering different shells (red lines) and (b) the corresponding inverse Fourier transforms (FT^{-1}) and the least-squares fits (red lines). (For interpretation of the references to colour in this figure legend, the reader is referred to the web version of this article.)

with the previously determined sorption isotherms as indicated in Figs. 1d and 5, respectively. The influence of carbonate is clearly shown by the decrease of the uranyl sorption down to log $R_d = 2.71$ L kg^{-1} for sample U_Mont3, compared to the carbonate free sample U_Mont1 with log $R_d = 4.02$ L kg^{-1} (see Table 4). The strong decrease in sorption with increasing carbonate concentration also indicates that no uranyl solid phase precipitated under the given experimental conditions.

From the sorption model calculations the surface speciation indicates that for the carbonate free sample U_Mont1, the neutral $\equiv S^{W1}OUO_2OH^0$ species on the weak sites is the dominant surface complex, representing ~100% of the sorbed U(VI) (Fig. 1d). For the samples U_Mont2 and U_Mont3 prepared in the presence of carbonate, the surface speciation indicates that the ternary uranyl mono-carbonate surface complexes ($\equiv S^{W1}OUO_2CO_3^-$) on the weak sites, is the dominant surface complex, representing ~100% of the sorbed U(VI) (Fig. 5). Surface complexation modelling suggests that under the used sample preparation conditions (pH ~8 and U(VI) loadings between 5 and 7 mmol kg^{-1}) sorption on strong sites is negligible and can probably not be assessed by EXAFS.

Fig. 6 shows the EXAFS spectra for the three U(VI) samples in the absence (U_Mont1) and presence of carbonate (U_Mont2 and U_Mont3). The three U loaded clay samples exhibit very similar χ functions and the corresponding radial structure functions (RSFs) display backscattering contributions at the same distances (peaks A to E) up to ~3.1 Å (R + ΔR). The RSFs are not corrected for phase shifts, Δ, causing peaks to appear at shorter distances relative to the real distance.

The EXAFS spectra of the three samples obtained at 35° were fitted in the *R*-space and the results of the data analysis are summarized in the Table 7. The different fit results are shown in Fig. 7 for U_Mont1 and in the Electronic annex Fig. EA2 for U_Mont2 and U_Mont3.

The derived structural parameters are identical for the three samples as already suggested by the similarity of the spectra. The first peak (A) was best fitted with an axial oxygen shell (O_{ax}) at a distance of 1.80 Å. The coordination number (CN) was obtained without constraining any fit parameter and varies between 2.1 and 2.2 which is consistent with the expected O_{ax} coordination.

Peak B and C could be fitted with two equatorial oxygen shells U–O_{eq1} and U–O_{eq2} with distances of ~2.30 Å and ~2.48 Å, respectively, and is consistent with a split of the equatorial oxygen shell. The shortened U–O_{eq1} distance of 2.30 Å compared to the distances between 2.41 Å and 2.43 Å obtained for outer-sphere uranyl aquo-complexes (Dent et al., 1992; Chisholm-Brause et al., 1994) and the splitting of the equatorial shell confirm the formation of an uranyl inner-sphere complex at the montmorillonite surface (Sylwester et al., 2000; Catalano and Brown, 2005; Schlegel and Descostes, 2009). The short U–O_{eq} distance of 2.3 Å corresponds to the mineral surface bond, whereas the longer distance of 2.48 Å represents the remaining equatorial oxygen atoms in contact with the aqueous phase. The sum of the CN of both equatorial oxygen shells was constrained to 6 for each sample.

Peak E at ~3.1 Å (R + ΔR), usually attributed to the multiple scattering (MS) paths of the uranyl moiety is more pronounced than normally observed in aqueous uranyl. Considering only the MS paths did not allow to fit this peak properly, indicating a superposition of MS effects of the U–O_{ax} shell, and single backscattering contribution from other atomic shells. To reproduce peak E, two different approaches reported in the literature were tested: (i) with a U–Si backscattering pair as suggested by Hennig et al. (2002) and Schlegel and Descostes (2009), and (ii) with a U-Fe backscattering pair as suggested by Catalano and Brown (2005). The latter authors investigated the sorption of U(VI) on SWy-1 (3.35 wt.% Fe_2O_3 (Van Olphen and Fripiat, 1979)) montmorillonite whereas the former authors, Hennig et al., studied an iron "poor" STx-1 (0.65 wt.% Fe_2O_3) montmorillonite. Peak E could be reproduced either with a U–Fe distance of 3.42 Å or with a U–Si/Al distance of 3.28 Å (EXAFS is unable to distinguish between Si and Al) as illustrated in Fig. 7. The fitted U–Si/Al distance is in a good agreement with a bidentate mononuclear coordination to one Al octahedra suggesting the formation of an edge sharing bidentate complex with Al octahedra at the montmorillonite edge sites. Similar U–Si/Al distances have been reported for montmorillonite (Schlegel and Descostes, 2009), kaolinite (Krepelova et al., 2008) and imogolite (Arai et al., 2006). The fitted U–Fe distance of 3.42 Å is in agreement with bidentate linkage of iron to the equatorial plane of U(VI) (Reich et al., 1998; Bargar et al., 2000; Rossberg et al., 2009) and would imply that U(VI) binds preferentially to Fe sites over Al sites as already observed by Catalano and Brown (2005). The fit quality with both approaches is quite good and does not allow to conclusively state which of both approaches is the best (Fig. 7).

However, the fit results could be further improved by considering an additional Al/Si shell at a short distance of ~3.09 Å, leading to a decrease of R_f and Red-χ by at least a factor of two. Including this short U–Al/Si shell allowed to reproduce peak D at ~2.7 Å (R + ΔR) and to obtain extremely good fit quality as suggested by the very low R_f and Red-χ values (see Table 7). The improvement of the fit is clearly evidenced in Fig. 7 and Fig. EA2. This short distance of ~3.09 Å lies within the values ranging from 3.08 to 3.16 Å reported for U(VI) sorbed on silica and albite, in boldwoodite, soddyite or in amorphous uranyl silicates, corresponding to a bidentate coordination of U(VI) to one Si atom (Demartin et al., 1992; Reich et al., 1996; Sylwester et al., 2000; Burns, 2005; Walter et al., 2005; Soderholm et al., 2008). The sorption of U(VI) on kaolinite (Krepelova et al., 2008) is the only study on a clay mineral for which this short U-Si/Al distance was reported. Fitting the entire spectra without this short U-Si/Al distance does not allow to reproduce the spectra as good and reduces strongly the fit quality (see Fig. 7).

The coordination number for the Al_1/Si_1, Al_2/Si_2 shells and/or Fe are quite low, varying between 0.9 and 1.3 (when considering two Al/Si shells) and between 0.3 and 0.8 (when considering one Al_1/Si_1 shell and one Fe shell) but are in a good agreement with the values reported in literature (Catalano and Brown, 2005; Schlegel and Descostes, 2009). The interference between the MS paths associated with O_{ax} and the single scattering paths can reduce the accuracy on the CN. No spectral features originating from a backscattering interaction were observed in the FT at $R > 3.5$ Å. No U–U interaction could be observed in the FT, indicating that no U(VI) solid phase precipitation occurred (also indicated by the sorption isotherm, Fig. 1d in Section 3.1) and that U(VI) is forming mononuclear complexes at the montmorillonite surface. The splitting of the equatorial oxygen shell and the identification of different backscattering pairs originating from the montmorillonite bulk structure (Al_1/Si_1 and Al_2/Si_2 or Fe) clearly indicates that under the given experimental conditions inner-sphere complexation at the clay surface occurs via binding to Al/Fe octahedral and/or Si tetrahedra.

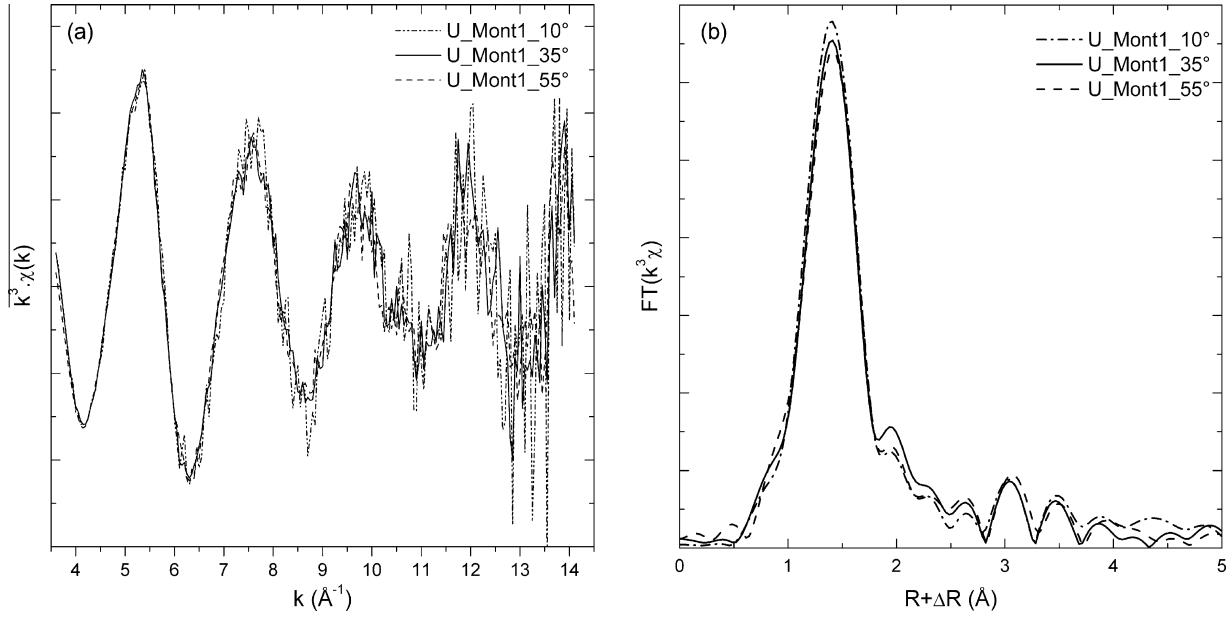

Fig. 8. (a) k^3-weighted spectra of the carbonate free sample U_Mont1 at the angles 10°, 35° and 55° and (b) the corresponding RSFs.

It is known from the literature that carbonate mainly binds in a bidentate fashion to uranyl in aqueous uranyl carbonate complexes, on carbonate solids such as aragonite but also in uranyl carbonates *e.g.* liebigite, cejkaite (Bargar et al., 2000; Catalano and Brown, 2004; Elzinga et al., 2004; Amayri et al., 2005; Kelly et al., 2007; Rossberg et al., 2009). The similarity of the EXAFS spectra of the carbonate free sample U_Mont1 and the samples U_Mont2 and U_Mont3 prepared in the presence of carbonate (Fig. 6) already indicated that there is no major difference between these samples and this is confirmed by the fit results (Table 7). No additional shells originating from a uranyl bidentate carbonate surface complex (U–C, U–O_{dist}), were necessary to reproduce the spectra of the samples prepared in the presence of carbonate. Fitting a C shell at ~2.9 Å instead of a Si decreased the fit quality of the spectra.

Fitting a light backscattering element such as carbon in the U_Mont2 and U_Mont3 spectra might be difficult since the backscattering amplitude originating from 1 C ($z = 6$) is much weaker than the amplitude originating from one Si/Al shell ($z = 13/14$). Catalano et al. (2005) postulated the formation of bidentate uranyl mono-carbonate complexes at the montmorillonite surface in the pH range 5.6–7.2 based on the fitted C shell at ~2.9 Å. However, no Si or Al shells originating from the clay surface were observed in the study of Catalano et al. (2005). The most reliable structural evidence for the formation of bidentate uranyl carbonate complexes at the montmorillonite surface would be the peak produced by the distal oxygen O_{dist} and the multiple scattering of U–C–O_{dis} and U–C–O_{dist}–C at ~3.7 Å ($R + \Delta R$) of the carbonate ligand (Rossberg et al., 2009). These features could not be observed in the spectra of our U(VI)-carbonate montmorillonite samples.

4.2. P-EXAFS: carbonate free sample U_Mont1

P-EXAFS measurements were carried out only on the carbonate free U_Mont1 at pH ~8. Fig. 8 shows the U L_{III} edge k^3-weighted spectra of the U_Mont1 at the angles 10°, 35° and 55° and the corresponding RSFs. The sample at an angle of 80° was not measured but can in principle be calculated by linear regression from the three others angles (Manceau et al., 1998). However, the P-EXAFS spectra of U-Mont1 sample do not show any significant differences indicating that there is only small to no angular dependency.

The small P-EXAFS dependency can be caused by U complexes sorbed close to a magic β angle of 54.7° to the montmorillonite surface, where the polarization dependence is independent of the α angles (Manceau et al., 1998). A further explanation is that the P-EXAFS dependency is in general smaller at the L_2- and L_3-edges, than at K- and L_1 edges (Hennig, 2006). This is caused by the fact that the P-EXAFS formula for samples with a preferred orientation for the L_2- and L_3-edges contains *s, d* and coupled *s-d* states. Whereas the dominant *d* contribution at the L_3-edge is running with $(1 + 3\cos^2\theta_{ij})$, its influence is attenuated by the s-d cross term running with $(1 - 3\cos^2\theta_{ij})$ in the opposite direction (Stern, 1988; Hennig, 2006). θ_{ij} is the angle between the electric field vector of the X-ray beam (ε) and the vector R_{ij} connecting the X-ray absorber to the i^{th} backscattering atom of the j^{th} shell. For a textured sample, such as self-supporting clay films θ can be expressed as a function of α and β angles, where α is the angle between ε and a selected plane (defined *e.g.* by two crystallographic axes) and β is the angle between R and the normal vector n of this plane) (for details see Citrin (1985), Hennig (2006), Schlegel and Descostes (2009)).

The three P-EXAFS spectra were fitted simultaneously, using a single value for E_0, and for a given shell, a common bond length and Debye–Waller factor. However, due to the noisy spectra obtained at 10°, the "simultaneously" investigable k range for the FT was reduced to 3.6–11.5 $Å^{-1}$.

The structural parameters derived from the multiple-shell fit in the R-space and the corresponding simulated FT^{-1} together with the experimental data, are given in the Electronic annex (Fig. EA3 and Table EA3). Again both approaches (Fe shell or Al/Si shell) were tested and give equally good fit results. Small differences in the derived structural parameters compared to the parameters summarized in Table 7 are due to the shorter k range.

The fit results for the P-EXAFS spectra of sample U_Mont1 (Table EA3) confirm the lack of a pronounced angular dependency since the CN number of the different backscatter shells are within the experimental errors constant. However, based on the good correlations between coordination numbers and $\cos^2\alpha$ (Electronic annex Fig. EA4) it can be assumed that the relative error of the CN is smaller than the absolute errors given in Table EA3. The simplified P-EXAFS equation for the L_{III}-edge, under the assumption of a perfectly textured sample was used to calculate β_j angles of the different backscattering shells,

$$\chi_j^{\alpha}(k) = \chi_j^{iso}(k)[0.45\cos^2\alpha(1 - 3\cos^2\beta_j) + (0.7 + 0.9\cos^2\beta_j]$$

where $\chi_j^{iso}(k)$ is the EXAFS contribution for a powder sample (see Electronic annex EA4 for detailed calculations).

This approach yielded for the fit solution with two Al/Si shells: β_{U-Oax} ~61°, β_{U-Oeq1} ~52°, β_{U-Oeq2} ~48°, $\beta_{U-Si1/Al1}$ ~40° and $\beta_{U-Si2/Al2}$ ~54° (similar values were obtained for the fit solution with U-Fe backscattering pairs). These values compare well to the one in the study of Schlegel and Descostes (2009) (β_{U-Oax} ~52°, β_{U-Oeq1} ~53°, β_{U-Oeq2} ~61° and $\beta_{U-Si2/Al2}$ ~60°). For U(VI) complexes bond to Al/Fe-octahedra one would expect $\beta_{U-Al/Fe}$ close to 90°. However, it should be noted that the small coordination numbers and angular dependency is strongly influenced by damping interferences between the single scattering U–Al/Si/Fe and the multiple scattering U–O_{ax} backscattering pairs, reducing significantly the accuracy of the β values (Hudson et al., 1996; Schlegel and Descostes, 2009). In addition, a discrepancy between theory and experimental data was observed by Hennig et al. (2006) investigating the polarization dependency at the L_1 and L_3 edges of uranium using a single crystal of $Ca[UO_2PO_4]_2{\cdot}6H_2O$. In this study a systematic deviation between experimental and theoretical CN of O_{ax} and O_{eq} with α were observed, which was attributed to an anisotropic Debye Waller factor.

Therefore, as suggested by Schlegel and Descostes (2009), β_{U-Oax} is the best suited angle to identify the sorption sites of U(VI) on the montmorillonite surface. The calculation yielded for the U–O_{ax} shell an angle of β_{U-Oax} ~60°, for the fit approach with an Al/Si or Fe shell, respectively. The β_{U-Oax} ~60° compares well with a theoretical value of 55°, if U is in the same plane as the Al and Fe atoms. Furthermore, this β_{U-Oax} corresponds to the magic angle of 54.7° for which CNs are independent of α. Therefore, based on the absence of a polarization dependence it seems likely that U(VI) forms edge surface complexes in the continuity of the octahedral sheets.

In contrary the finding of a short and long U-Al/Si distance could also suggest that uranium forms inner-sphere complexes by edge sharing with aluminum/iron octahedra and /or silicon tetrahedra. Similar observations were made by Krepelova et al. (2008) investigating the uptake of U(VI) by kaolinite. The results of the P-EXAFS measurements suggest that under the used experimental conditions a series of surface complexes in which U(VI)-polyhedra bridge to the montmorillonite surface exist, in such a manner that the polarization effect is levelled out.

4.3. Bond valence analysis of potential binding sites

The stability of U(VI) surface complexes on the various functional groups using the bond valence method (Pauling, 1929) were evaluated, in order to further constrain the possible binding geometries of U(VI) on the montmorillonite edge sites. This method has been applied on many occasions to assess the relative stabilities of surface sites and surface complexes on different minerals (for details see *e.g.* Bargar et al. (1997), Arai et al. (2006), Catalano et al. (2005)).

Details on the bond valence calculations and the bond valences obtained for the montmorillonite surface groups and the potential U(VI) surface complexes are given in the Electronic annex EA5.

From the bond valence calculations, surface complexation via binding to two Al/Fe octahedra *i.e.* $(Al/Fe)_2$–O–UO_2 seems to be a less plausible conformation. The most stable bonding are predicted for the surface complexes Si–O–UO_2, Al/Fe–OH–UO_2 and Al/FeSi–O–UO_2 depending on whether they are accepting H bonds or not. These conformations are in a good agreement with binding to Al/Fe octahedra and/or Si tetrahedra, however do not allow to state where U(VI) sorbs preferentially.

5. SUMMARY AND CONCLUSION

Determining the fate of uranium and the processes affecting transport, especially sorption onto mineral surfaces, under geological relevant conditions is essential in order to develop predictive sorption models. In this study, macroscopic sorption experiments, modelling, EXAFS measurements and bond valence calculations were carried out to investigate the uptake of U(VI) on montmorillonite in the absence and presence of carbonate.

5.1. Sorption experiments and modelling

The uptake of U(VI) on Na-SWy-1 was quantified by means of sorption experiments carried out under different experimental conditions (pH, pCO_2, U(VI) concentration). The sorption edges and isotherms obtained were successfully reproduced using the 2SPNE SC/CE sorption model. Two ternary uranyl-carbonate surface complexes on the strong sites ($\equiv S^SOUO_2CO_3^-$ and $\equiv S^SOUO_2(CO_3)_2^{3-}$) and one on the weak sites ($\equiv S^{W1}OUO_2CO_3^-$) were required to model the data obtained in the presence of carbonate. The fact that the same set of surface complexation reactions and constants could be used to reproduce the measurements made under a wide range of conditions provided additional confidence in the modelling.

5.2. Structure of U(VI) sorbed on SWy-1

EXAFS measurements confirmed that U(VI) forms inner-sphere complexes at the montmorillonite surface under the chosen experimental conditions. The best fit to the EXAFS oscillations measured for the U(VI) montmorillonite system was obtained with a structural model consisting of three uranium–oxygen coordination shells (*i.e.* U–O_{ax} at 1.80 Å, U–O_{eq1} at ~2.30 Å and U–O_{eq2} at ~2.48 Å), one Al/Si shell at ~3.09 Å and one Al/Si shell at ~3.29 Å or one Fe shell at ~3.42 Å. A preferential sorption either to the Al octahedra or Si tetrahedra edge sites could not be discriminated and coupling the EXAFS and P-EXAFS results suggests that U(VI) sorbs on the montmorillonite edge sites through binding to octahedral Al/Fe and/or tetrahedral Si.

Even though the modelling of the experimental sorption data in the presence of carbonate clearly indicated the formation of U(VI)-carbonate surface complexes, this could not be verified by the EXAFS measurements. Adding a U–C shell at ~2.9 Å had no significant influence on the quality of the fit to the spectra and the structural parameters obtained, indicating that EXAFS might be not sensitive enough to detect U-C shells in clay systems where elements with stronger backscattering amplitudes than carbon are present.

ACKNOWLEDGEMENT

We would like to thank Astrid Schaible and Vanessa Kalbermatter for technical assistance and the Rossendorf Beamline Staff (ESRF, Grenoble) for their great support during EXAFS measurement campaign. The European Commission is gratefully acknowledged for financial support under the project JP 06-02 of the ACTINET Network of Excellence, and in the frame of the Intra-European Fellowship FP6-036420. Partial financial support was provided by the National Cooperative for the Disposal of Radioactive Waste, Nagra (Switzerland).

APPENDIX A. SUPPLEMENTARY DATA

Supplementary data associated with this article can be found, in the online version, at http://dx.doi.org/10.1016/j.gca.2012.04.017.

REFERENCES

Amayri S., Reich T., Arnold T., Geipel G. and Bernhard G. (2005) Spectroscopic characterization of alkaline earth uranyl carbonates. *J. Solid State Chem.* **178**(2), 567–577.

Ankudinov A. L., Ravel B., Rehr J. J. and Conradson S. D. (1998) Real-space multiple-scattering calculation and interpretation of x-ray-absorption near-edge structure. *Phys. Rev. B* **58**(12), 7565.

Arai Y., McBeath M., Bargar J., Joye J. and Davis J. (2006) Uranyl adsorption and surface speciation at the imogolite–water interface: self-consistent spectroscopic and surface complexation models. *Geochim. Cosmochim. Acta* **70**(10), 2492–2509.

Bachmaf S., Planer-Friedrich B. and Merkel B. J. (2008) Effect of sulfate, carbonate, and phosphate on the uranium (VI) sorption behavior onto bentonite. *Radiochim. Acta* **96**(6), 359–366.

Bacmann M. and Bertaut E. F. (1967) Structure du nouveau compose $UFeO_4$. *Bull. Soc. fr. Miner. Cristallogr.* **90**, 257–258.

Baeyens B. and Bradbury M. H. (1995a) A quantitative mechanistic description of Ni, Zn and Ca sorption on Na-montmorillonite. Part I: Physico-Chemical Characterization and Titration Measurements, PSI Bericht Nr. 95–10, Villigen PSI, Switzerland.

Baeyens B. and Bradbury M. H. (1995b) A quantitative mechanistic description of Ni, Zn and Ca sorption on Na-montmorillonite. Part II: Sorption Measurments, PSI Bericht Nr. 95–11, Villigen PSI, Switzerland.

Baeyens B. and Bradbury M. H. (1997) A mechanistic description of Ni and Zn sorption on Na- montmorillonite.1. Titration and sorption measurements. *J. Contam. Hydrol.* **27**(3–4), 199–222.

Baeyens B. and Bradbury M. H. (2004) Cation exchange capacity measurements on illite using the sodium and cesium isotope dilution technique: effects of the index cation, electrolyte concentration and competition: modeling. *Clays Clay Miner.* **52**(4), 421–431.

Bargar J. R., Towle S. N., Brown, Jr, G. E. and Parks G. A. (1997) XAFS and bond-valence determination of the structures and compositions of surface functional groups and Pb(II) and Co(II) sorption products on single-crystal α-Al_2O_3. *J. Colloid Interface Sci.* **185**(2), 473–492.

Bargar J. R., Reitmeyer R., Lenhart J. J. and Davis J. A. (2000) Characterization of U(VI)-carbonato ternary complexes on hematite: EXAFS and electrophoretic mobility measurements. *Geochim. Cosmochim. Acta* **64**(16), 2737–2749.

Bond D. L., Davis J. A. and Zachara J. M. (2007) Uranium(VI) release from contaminated vadose zone sediments: estimation of potential contributions from dissolution and desorption. In *Adsorption of Metals to Geomedia II: Variables, Mechanisms, and Model Applications* (eds. M. O. Barnett and D. B. Kent). Elsevier.

Bradbury M. H. and Baeyens B. (1997) A mechanistic description of Ni and Zn sorption on Na- montmorillonite. 2. Modelling. *J. Contam. Hydrol.* **27**(3–4), 223–248.

Bradbury M. H. and Baeyens B. (2005) Modelling the sorption of Mn(II), Co(II), Ni(II), Zn(II), Cd(II), Eu(III), Am(III), Sn(IV), Th(IV), Np(V) and U(VI) on montmorillonite: linear free energy relationships and estimates of surface binding constants for some selected heavy metals and actinides. *Geochim. Cosmochim. Acta* **69**(22), 875–892.

Burns P. C. and Finch R. (1999) Uranium: mineralogy, geochemistry and the environment. *Rev. Mineral.* (Washinton DC).

Burns P. C. (2005) U6+ minerals and inorganic compounds: insight into an expanded structural hierarchy of crystal structures. *Can. Mineral.* **43**, 1839–1894.

Catalano J. G. and Brown, Jr., G. E. (2004) Analysis of uranyl-bearing phases by EXAFS spectroscopy: Interferences, multiple scattering, accuracy of structural parameters, and spectral differences. *Am. Mineral.* **89**(7), 1004–1021.

Catalano J. G. and Brown G. E. (2005) Uranyl adsorption onto montmorillonite: Evaluation of binding sites and carbonate complexation. *Geochim. Cosmochim. Acta* **69**(12), 2995–3005.

Catalano J. G., Trainor T. P., Eng P. J., Waychunas G. A. and Brown, Jr, G. E. (2005) CTR diffraction and grazing-incidence EXAFS study of U(VI) adsorption onto α-Al_2O_3 and α-Fe_2O_3 (1102) surfaces. *Geochim. Cosmochim. Acta* **69**(14), 3555–3572.

Chisholm-Brause C., Conradson S. D., Buscher C. T., Eller P. G. and Morris D. E. (1994) Speciation of uranyl sorbed at multiple binding sites on montmorillonite. *Geochim. Cosmochim. Acta* **58**(17), 3625–3631.

Citrin P. H. (1985) Bond lengths and coordination numbers from $L_{2,3}$-edge versus K-edge surface extended x-ray-absorption fine structure. *Phys. Rev. B* **31**(2), 700–721.

Demartin F., Gramaccioli C. M. and Pilati T. (1992) The importance of accurate crystal-structure determination of uranium minerals. 2. Soddyite $(UO_2)2(SiO_4).2H_2O$. *Acta Crystallogr. Sect. C Cryst. Struct. Commun.* **48**, 1–4.

Dent A. J., Ramsay J. D. F. and Swanton S. W. (1992) An EXAFS study of uranyl ion in solution and sorbed onto silica and montmorillonite clay colloids. *J. Colloid Interface Sci.* **150**(1), 45–60.

Elzinga E. J., Tait C. D., Reeder R. J., Rector K. D., Donohoe R. J. and Morris D. E. (2004) Spectroscopic investigation of U(VI) sorption at the calcite-water interface. *Geochim. Cosmochim. Acta* **68**(11), 2437–2448.

Finch R. J., Cooper M. A., Hawthorne F. C. and Ewing R. C. (1999) Refinement of the crystal structure of rutherfordine. *Can. Mineral.* **37**(4), 929–938.

Guillaumont R., Fanghänel T., Fuger J., Grenthe I., Neck V., Palmer D. A. and Rand M. H. (2003) *Update on the Chemical Thermodynamics of Uranium, Neptunium, Plutonium, Americium and Technetium*. Elsevier, Amsterdam.

Hennig C., Reich T., Dähn R. and Scheidegger A. M. (2002) Structure of uranium sorption complexes at montmorillonite edge sites. *Radiochim. Acta* **90**(9–11), 653–657.

Hennig C. (2006) Polarization effects in EXAFS spectra at the uranium L1 and L3 edge – a comparison between theory and experiment. In *Recent Advances in Actinide Science* (eds. I. May, R. Alvarez and N. Bryan). RCS Publishing, The Royal Society of Chemistry, Cambridge, pp. 716–718.

Hudson E. A., Allen P. G., Terminello L. J., Denecke M. A. and Reich T. (1996) Polarized x-ray-absorption spectroscopy of the uranyl ion: comparison of experiment and theory. *Phys. Rev. B* **54**(1), 156.

Kelly S. D., Kemner K. M. and Brooks S. C. (2007) X-ray absorption spectroscopy identifies calcium-uranyl-carbonate complexes at environmental concentrations. *Geochim. Cosmochim. Acta* **71**(4), 821–834.

Kim S. (2001) Sorption mechanism of U(VI) on a reference montmorillonite: binding to the internal and external surfaces. *J. Radioanal. Nucl. Chem.* **250**(1), 55–62.

Kowal-Fouchard A., Drot R., Simoni E. and Ehrhardt J. J. (2004) Use of spectroscopic techniques for uranium(VI)/montmorillonite interaction modeling. *Environ. Sci. Technol.* **38**(5), 1399–1407.

Krepelova A., Reich T., Sachs S., Drebert J. and Bernhard G. (2008) Structural characterization of U(VI) surface complexes on kaolinite in the presence of humic acid using EXAFS spectroscopy. *J. Colloid Interface Sci.* **319**(1), 40–47.

Manceau A., Chateigner D. and Gates W. P. (1998) Polarized EXAFS, distance-valence least-squares modeling (DVLS), and quantitative texture analysis approaches to the structural

refinement of Garfield nontronite. *Phys. Chem. Miner.* **25**(5), 347–365.

McKinley J. P., Zachara J. M., Smith S. C. and Turner G. D. (1995) The influence of uranyl hydrolysis and multiple site-binding reactions on adsorption of U(VI) to montmorillonite. *Clays Clay Miner.* **43**(5), 586–598.

Nagra (2002), Project Opalinus Clay: Safety Report. Demonstration of disposal feasibility (Entsorgungsnachweis) for spent fuel, vitrified high-level waste and long-lived intermediate-level waste, Technical Report NTB 02–05, Wettingen, Switzerland.

Newville M., Livins P., Yacoby Y., Rehr J. J. and Stern E. A. (1993) Near-edge X-ray-absorption fine structure of Pb: a comparison of theory and experiment. *Phys. Rev. B* **47**(21), 14126.

Newville M. (2001) EXAFS analysis using FEFF and FEFFIT. *J. Synchrotron Radiat.* **8**, 96–100.

Pabalan R. T. and Turner D. R. (1997) Uranium(6+) sorption on montmorillonite: experimental and surface complexation modeling study. *Aquat. Geochem.* **2**(3), 203–226.

Pauling L. (1929) The principles determining the structure of complex ionic crystals. *J. Am. Chem. Soc.* **51**(4), 1010–1026.

Perrin and Dempsey (1974) *Buffers for pH and Metal Ion Control*. Chapmann and Hall, London.

Ravel B. and Newville M. (2005) ATHENA, ARTEMIS, HEPHAESTUS: data analysis for X-ray absorption spectroscopy using IFEFFIT. *J. Synchrotron Radiat.* **12**, 537–541.

Rehr J. J., Mustre de Leon J., Zabinsky S. I. and Albers R. C. (1991) Theoretical x-ray absorption fine structure standards. *J. Am. Chem. Soc.* **113**(14), 5135–5140.

Reich T., Moll H., Denecke M. A., Geipel G., Bernhard G. and Nitsche H. (1996) Characterization of hydrous uranyl silicate by EXAFS. *Radiochim. Acta* **74**, 219–223.

Reich T., Moll H., Arnold T., Denecke M. A., Hennig C., Geipel G., Bernhard G., Nitsche H., Allen P. G., Bucher J. J., Edelstein N. M. and Shuh D. K. (1998) An EXAFS study of uranium(VI) sorption onto silica gel and ferrihydrite. *J. Electron. Spectrosc. Relat. Phenom.* **96**(1–3), 237–243.

Rossberg A., Ulrich K.-U., Weiss S., Tsushima S., Hiemstra T. and Scheinost A. C. (2009) Identification of Uranyl Surface Complexes on Ferrihydrite: advanced EXAFS Data Analysis and CD-MUSIC Modeling. *Environ. Sci. Technol.* **43**(5), 1400–1406.

Schlegel M. L., Manceau A., Charlet L., Chateigner D. and Hazemann J.-L. (2001) Sorption of metal ions on clay minerals. III. Nucleation and epitaxial growth of Zn phyllosilicate on the edges of hectorite. *Geochim. Cosmochim. Acta* **65**(22), 4155–4170.

Schlegel M. L. and Descostes M. (2009) Uranium Uptake by Hectorite and Montmorillonite: A Solution Chemistry and Polarized EXAFS Study. *Environ. Sci. Technol.* **43**(22), 8593–8598.

Soderholm L., Skanthakumar S., Gorman-Lewis D., Jensen M. P. and Nagy K. L. (2008) Characterizing solution and solid-phase amorphous uranyl silicates. *Geochim. Cosmochim. Acta* **72**(1), 140–150.

Sposito G. (1984) *The Surface Chemistry of Soils*. Oxford University Press, New York.

Stern E. A. (1988) Theory of EXAFS. In *X-ray Absorption: Principles, Applications, Techniques of EXAFS, SEXAFS and XANES* (eds. D. C. Konigsberger and R. Prins). John Wiley & Sons.

Stern E. A. (1993) Number of relevant independent points in x-ray-absorption fine-structure spectra. *Phys. Rev. B* **48**(13), 9825.

Sylwester E. R., Hudson E. A. and Allen P. G. (2000) The structure of uranium (VI) sorption complexes on silica, alumina, and montmorillonite. *Geochim. Cosmochim. Acta* **64**(14), 2431–2438.

Turner G. D., Zachara J. M., McKinley J. P. and Smith S. C. (1996) Surface-charge properties and UO_2^{2+} adsorption of a subsurface smectite. *Geochim. Cosmochim. Acta* **60**(18), 3399–3414.

Van Olphen H. and Fripiat J. J. (1979) *Data Handbook for Clay Materials and Other Non-metallic Minerals*. Pergamon, New York.

Vespa M., Lanson M. and Manceau A. (2010) Natural attenuation of zinc pollution in smelter-affected soil. *Environ. Sci. Technol.* **44**(20), 7814–7820.

Walter M., Arnold T., Geipel G., Scheinost A. and Bernhard G. (2005) An EXAFS and TRLFS investigation on uranium(VI) sorption to pristine and leached albite surfaces. *J. Colloid Interface Sci.* **282**(2), 293–305.

Westall J., Zachary J. L. and Morel F. (1976) MINEQL, A Computer Program for the Calculation of Chemical Equilibrium Composition of Aqueous Systems. Technical Note 18, Cambridge, Massachusetts.

Zachara J. M. and McKinley J. P. (1993) Influence of hydrolysis on the sorption of metal cations by smectites: Importance of edge coordination reactions. *Aquat. Sci.* **55**(4), 250–261.

Associate editor: Jacques Schott